Catalysis Today 216 (2013) 24–29

Contents lists available at SciVerse ScienceDirect

Catalysis Today

journal homepage: www.elsevier.com/locate/cattod

Novel catalytic ceramic papers applied to oxidative dehydrogenation of ethane

J.P. Bortolozzi, E.D. Banús, D. Terzaghi, L.B. Gutierrez, V.G. Milt, M.A. Ulla*

Instituto de Investigaciones en Catálisis y Petroquímica, INCAPE (FIQ, UNL–CONICET), Santiago del Estero 2829, 3000 Santa Fe, Argentina

ARTICLE INFO

Article history:
Received 19 February 2013
Received in revised form 15 May 2013
Accepted 19 May 2013
Available online 10 July 2013

Keywords:
Catalytic ceramic papers
Nickel oxide
Nickel–cerium oxides
Oxidative dehydrogenation of ethane

ABSTRACT

The aim of this work was the development of novel structured catalysts applied to the oxidative dehydrogenation of ethane. Different Ni-based catalytic formulations promoted with cerium were incorporated onto ceramic papers and were tested in the reaction. Ceramic papers presented an interconnected 3D-network of silica–alumina fibers almost totally covered by the binder agent (Al_2O_3) and provided an adequate environment for the deposition of the catalyst. The catalytic results indicated that the paper with Ce/Ni = 0.17 atomic ratio showed the highest ethylene productivity, due to the presence of the smallest crystalline domain size of NiO and the partial incorporation of the Ni cation into the ceria lattice.

1. Introduction

Structured catalysts are currently used in many chemical reactions [1] because they show numerous advantages compared with conventional ones [2]. They are usually constituted by a catalytic coating onto a substrate, which can be formed by structures such as monoliths, meshes and foams, built with different materials (cordierite, stainless steel, metals) [3,4].

Ceramic papers constitute a novel kind of substrates, formed by linking fibers that produce a three-dimensional structure. This feature allows adapting them to diverse geometries thus presenting flexibility, versatility and easiness of handling, among other advantages [5]. By adding catalytic components to a ceramic paper, a structured catalyst can be obtained. The unique fiber-network microstructure with connected "pores" spaces provide a favorable reaction environment to promote desirable gas diffusion within the catalyst layer [6]. The principal characteristics of these structured catalytic reactors in comparison to conventional fixed bed reactor are lower pressure drop, shorter diffusional distances and higher geometric surfaces. In addition, the flow regime is turbulent allowing a better mixing of reagents and more uniform temperature profiles, preventing the generation of "hot spots". Since the oxidative dehydrogenation of ethane is an exothermic reaction, the last two characteristics are useful.

The use of catalytic papers has been reported for different reactions such as autothermal reforming (ATR) of methanol [7], toluene removal from a gas stream [8] and photocatalytic elimination of water pollutants [9]. Ceramic papers have also been used in the NO_X reduction with methane for the treatment of combustion gases [10] and the catalytic combustion of soot [11]. In the former reaction, the paper-structured catalyst demonstrated higher efficiency and more rapid thermal responsiveness than a conventional honeycomb catalyst, indicating that the paper-like structure contributes to effective transport of heat and reactants to the catalyst surfaces, even at low temperatures.

In addition, modifications in the preparation process such as the incorporation of silicon carbide lead to a better energy transfer and enhance the heat distribution, which is useful for exothermal reactions like methanol steam reforming (MSR) to produce hydrogen for fuel cells [12].

On the other hand, rare earth oxides have been largely investigated in catalysis as structural and electronic promoters in order to improve the activity, selectivity and thermal stability of the catalysts. Among them, the most outstanding one is cerium oxide because it is a key compound in two significant catalytic processes, three way catalysts (TWC) and fluid catalytic cracking (FCC). The significance of this oxide can be appreciated in numerous scientific publications and industrial patents. Distinctive chemical features as the redox ability in the presence of transition metals make CeO_2 an interesting compound to be employed in catalytic formulations [13]. The important role played by ceria is related to the generation and participation of surface oxygen species and anionic vacancies which could be modified by the presence of other elements into

* Corresponding author. Tel.: +54 342 4536861; fax: +54 342 4536861.
E-mail address: mulla@fiq.unl.edu.ar (M.A. Ulla).

0920-5861/$ – see front matter © 2013 Elsevier B.V. All rights reserved.
http://dx.doi.org/10.1016/j.cattod.2013.05.022

the lattice [14]. Specifically, the mixture of cerium and nickel has been investigated for many catalytic reactions such as nitrogen oxides reduction [15], methane total oxidation [16] and oxidative dehydrogenation of propane [17], among others.

Nickel-based materials are promising catalysts for the oxidative dehydrogenation reactions (ODE) because they have the capability of activating light paraffins at relatively low temperatures [18]. The ODE reaction is an interesting route for producing ethylene, a key intermediate for polyethylene and polyvinyl chloride (PVC) manufacturing. Current production processes employ high operating temperatures, resulting in increasing energy consumption. This reaction is exothermic and thermodynamic constraints are not present, which allows obtaining a better global energy balance.

In this context, the aim of this work was to investigate the feasibility of obtaining Ni and Ni–Ce catalysts incorporated to ceramic papers and to analyze, for the first time, the application of these novel structured catalysts on the oxidative dehydrogenation of ethane, used as test reaction. The systems were characterized by scanning electron microscopy (SEM), X-ray diffraction (XRD) and laser Raman spectroscopy (LRS).

2. Materials and methods

2.1. Preparation of ceramic and catalytic papers

Ceramics papers were prepared using a papermaking technique with a dual polyelectrolyte retention system which employs cationic and anionic polymers. This method improves the components retention during the paper manufacturing [19]. The incorporation of a binder to give mechanical resistance to the final ceramic paper is also required.

Fig. 1 shows a schematic preparation procedure of the catalytic ceramic papers. In order to obtain the ceramic paper, two kinds of materials were used: ceramic and cellulosic fibers. Further details were reported in a previous work [11]. In brief, a suspension was prepared with 1 L solution of NaCl (0.01 N) and 66 ml of the cationic polyelectrolyte (polyvinyl amine-PVAm-Luredur PR 8095, BASF). Dry ceramic fibers (48 wt% Al_2O_3 and 50 wt% SiO_2) (10 g) were added to the stirring suspension. The following step was the incorporation of 10 g of a binder agent (alumina colloidal suspension – Nyacol® AL20DW), 42 ml of the anionic polyelectrolyte (anionic polyacrylamide-A-PAM-Aquatec) and 1.5 g of cellulosic fiber (bleached softwood kraft pulp). With this suspension, sheets were produced by applying pressure using the SCAN standard method [20]. The sheets were dried at 25 °C during 24 h and calcined in a muffle at 550 °C during 2 h (1 °C/min). The ceramic papers so obtained were designated as PA.

To obtain catalytic papers, the ceramic papers (PA) were cut in ~20 mm diameter pieces. These pieces were placed over a plastic mesh and moistened up to saturation with solutions of either nickel nitrate or nickel and cerium nitrates with cerium/nickel atomic ratios being 0.05, 0.11, 0.17 and 0.25 and then calcined in air at 550 °C during 2 h. The structured catalysts so obtained were designated as Ni–PA and NiCe (*x*)–PA, where *x* is the cerium/nickel atomic ratio in the impregnation solution.

2.2. Characterization of ceramic and catalytic papers

The morphology and the components distribution of the papers obtained were analyzed by scanning electron microscopy (SEM) JEOL JSM-35C operating at 20 kV, equipped with EDX energy-dispersive system. The sample coating procedures were performed using a combined gold/carbon deposition of metals SPI supplies 12157-AX under argon atmosphere.

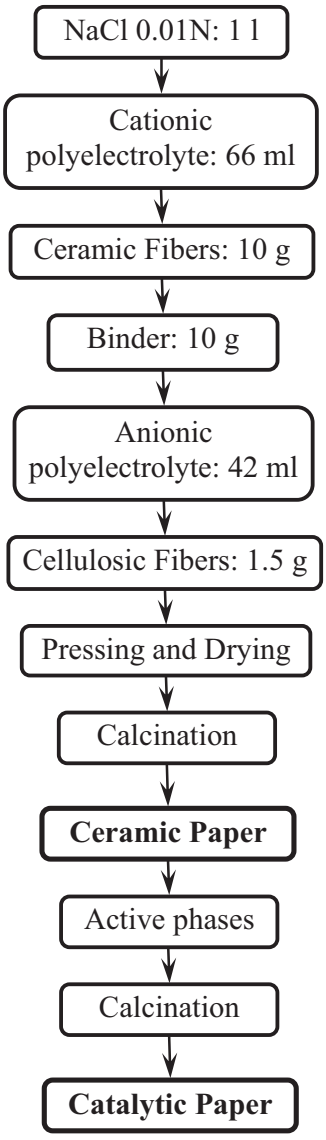

Fig. 1. Scheme of the preparation procedure of ceramic and catalytic papers.

Crystalline phases of the different catalytic papers were studied by X-ray diffraction (XRD). The analysis was performed with a Shimadzu XD-D1 diffractometer. Diffraction patterns were recorded using Cu-Kα radiation over a 20–85° range at a scan rate of 2°/min, operating at 30 kV and 40 mA. The pieces (disks with 20 mm of diameter) were supported in a special sample holder designed for the XRD analysis. The software package of the equipment was used for the identification of the phases. The size of nickel and cerium oxides crystallites were calculated by the Scherrer equation.

The plane used for the calculation of the crystallite size of nickel oxide was (2 0 0) corresponding to main peak of NiO at 43.3°. Whereas, for this calculation of cerium oxide, the plane (1 1 1) corresponding to main peak of CeO_2 at 28.6°. The calculated values are an average of two FWHM measurements of the corresponding peaks in different XRD patterns.

The Raman (LRS) spectra were recorded using a LabRam spectrometer (Horiba-Jobin-Yvon) coupled to an Olympus confocal microscope (a 100× objective lens was used for simultaneous illumination and collection), equipped with a CCD detector cooled to about −70 °C using the Peltier effect. The excitation wavelength was in all cases 532.13 nm (Spectra Physics diode pump solid state laser). The laser power was set at 30 mW.

2.3. Catalytic tests

The oxidative dehydrogenation of ethane was carried out in a flow system in a temperature range between 300 and 450 °C. The feed composition was 6% O_2 and 6% C_2H_6 diluted in He. Four catalytic paper disks ($\varnothing \approx 20$ mm) were stacked in the middle of a quartz reactor. Each catalytic paper disk contained about 18.1 ± 1.7 mg of active phases coated on ceramic fibers. Consequently, the total mass of metal oxides (MO: NiO, NiO–CeO_2) corresponding to the stacked four disks was ~70 mg. The gas flow was fixed to get a constant W/F value of 0.08 g s/cm^3, where W refers to the total weight of metal oxides (MO).

Reactants and products were analyzed with a Shimadzu GC 2014 gas chromatograph equipped with a packed column (HayeSep D®). Closure of the carbon mass balance was $100 \pm 2\%$. Carbon monoxide was not detected in the products stream after the reaction. The ethane conversion ($X_{C_2H_6}$) and the selectivity toward ethylene ($S_{C_2H_4}$) were based on the carbon mass balance and were calculated as follows:

$$X_{C_2H_6}(\%) = \frac{[CO] + [CO_2] + 2[C_2H_4]}{2[C_2H_6]} \times 100$$

$$S_{C_2H_4}(\%) = \frac{2[C_2H_4]}{[CO] + [CO_2] + 2[C_2H_4]} \times 100$$

The productivity of ethylene was given by the following equation:

$$P = \frac{F_{C_2H_6} \times X_{C_2H_6} \times S_{C_2H_4} \times M_{C_2H_4}}{W_{Ni}} \left(g_{ethylene}/kg_{Ni}\,h\right)$$

where $F_{C_2H_6}$ is the flow rate of ethane (mol/h), $M_{C_2H_4}$ is the molecular mass of ethylene (28 g/mol) and W_{Ni} is the mass of nickel (kg_{Ni}).

3. Results and discussion

3.1. Structural and morphological features of the papers

Before calcination, the sheet containing pulp and ceramic fibers presented a typical packed structure. The thickness of the final sheets was 1–2 mm approximately (Fig. 2a). During the thermal treatment, the cellulosic fibers were burned and the silica–alumina fibers formed an interconnected 3D-network. The structure presents high macroporosity as shown by the SEM micrographs (Fig. 2b). Besides, these fibers were almost completely covered by alumina particles with nanometric sizes (Fig. 2b), although there were some sectors without any coverage (Fig. 2c). The thickness of the layer was approximately 100–200 nm (estimated by cross section SEM micrographs) with an average size of alumina particles (aggregates) of 50–70 nm (Fig. 2d). The appearance of the final structure was similar to a flexible board.

After the addition of active phases, well-adhered catalyst particles spread all over the fibers structure were observed (Fig. 3a). The average size of these particles was lower than 1 μm and the predominant shape was almost spherical (Fig. 3b).

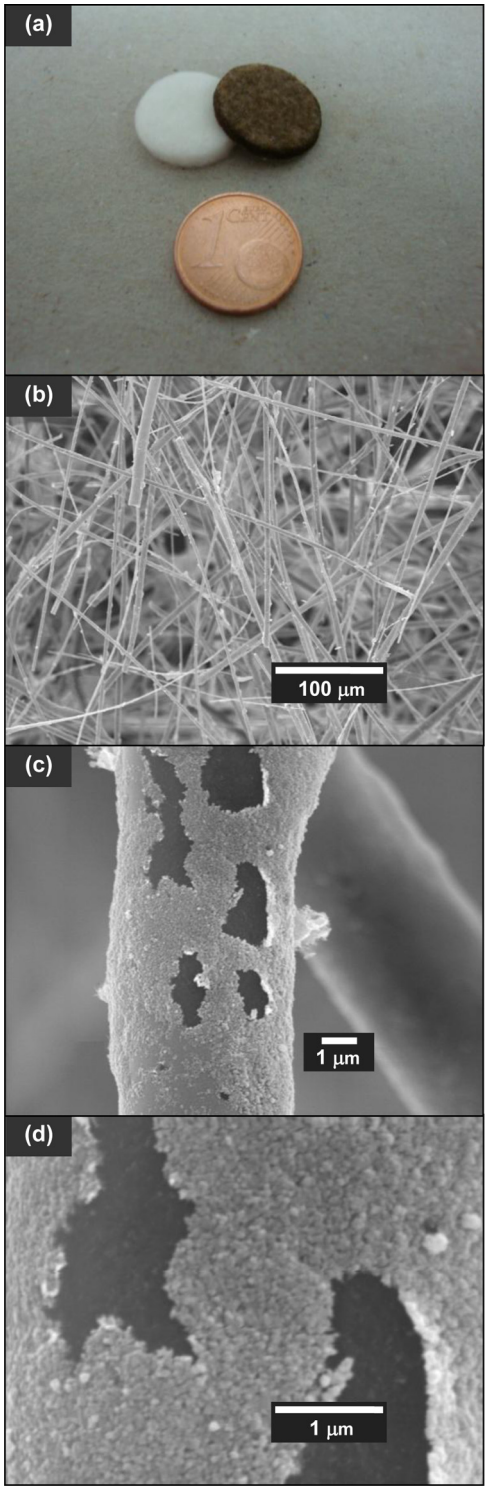

Fig. 2. SEM micrographs of the papers: ceramic paper (white disk, left) and catalytic paper (dark disk, right) (a), microstructure (b), fibers coverage (c) and coverage morphology (d).

3.2. Physicochemical characterization: active phases

Fig. 4 shows the XRD patterns of the catalysts. Characteristic peaks of nickel oxide (JCPDS: 47-1049; $2\theta = 37.3°, 43.3°, 62.9°, 75.5°$ and 79.6°) and cerium oxide (JCPDS: 43-1002; $2\theta = 28.6°$, 33.1°, 47.5°, 56.4°, 59.1°, 69.5°, 76.8° and 79.1°) were identified.

The peaks corresponding to the ceria phase were barely visible in NiCe (0.05)–PA but were better defined in the other cerium-promoted samples. These signals become sharper while the cerium content increase, which denotes higher ceria crystallinity. The crystallite size of ceria was estimated in 6.3, 7.4 and 8.8 nm for NiCe (0.11)–PA, NiCe (0.17)–PA and NiCe (0.25)–PA, respectively.

NiO crystallite sizes were estimated in 18.1, 14.5, 12.1, 10.7 and 12.9 nm for Ni–PA, NiCe (0.05)–PA, NiCe (0.11)–PA, NiCe (0.17)–PA and NiCe (0.25)–PA, respectively, showing that the presence of a certain amount of cerium inhibits the crystalline domain growth of nickel oxide, as reported by Solsona et al. [21].

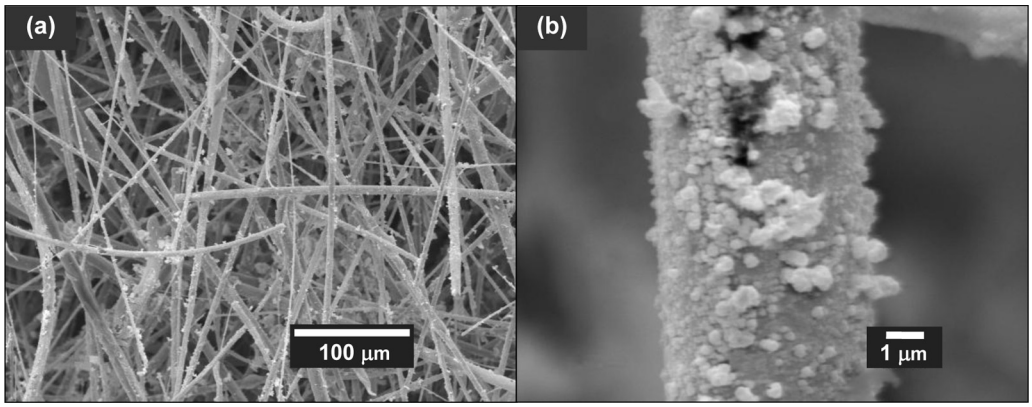

Fig. 3. SEM micrographs of the catalytic paper: structure (a) and catalytic particles detail (b).

The lower Ni^{2+} ionic radius (0.69 Å) [22] compared with Ce^{4+} (0.97 Å) [23] would allow a part of the nickel to be incorporated into the ceria, leading to the modification of the lattice parameters, as reported by Shan et al. and Deraz et al. [24,25].

Raman spectra of the catalysts presented an asymmetric and broad band corresponding to the stretching of the Ni–O bond (first order phonons) at ~500 cm^{-1} (Fig. 5). This signal suggests the presence of bulk NiO in agreement with the X-ray diffraction patterns. A shoulder associated with material surface vacancies was also observed at ~400 cm^{-1}. Besides, two very weak bands at 700 and 1080 cm^{-1} assigned to second order phonons (2TO and 2LO) of NiO were present. No significant shift in the frequency of the main signal was observed in Ni–PA, indicating that the nickel–alumina interaction (alumina from the fibers coverage) was weak.

On the other hand, the ceria fluorite-type structure presents a sharp band located at 460–465 cm^{-1} corresponding to the F2g mode of cerium oxide (oxygen atoms vibrating around the Ce^{4+} cation) [26]. Indeed, the Raman spectrum of the cerium-paper (without nickel oxide) presents this main band at 465 cm^{-1}.

The spectra of the Ce-containing catalysts showed this characteristic signal of CeO_2 although a marked shift (~5–10 cm^{-1}) was observed. In all spectra, this signal shifted to lower frequencies, suggesting a distortion in the ceria structure. This shift of the main band followed a general trend: catalysts with higher amount of cerium shifted less than formulations with lower amount of the promoter (Fig. 5 inset).

Additionally, an extra band at 224 cm^{-1} and a small shoulder at ~630 cm^{-1} associated with strong modifications in the oxygen network were also identified [18]. Moreover, the Ni–O stretching band in the Ce-promoted catalysts was notoriously shifted to higher frequencies (~60–70 cm^{-1}) on these spectra. These latter observations confirm that the incorporation of the Ni cation into the ceria lattice took place up to some extent, producing modifications in the oxygen lattice. This lattice alteration would generate new species for the ethane oxydehydrogenation and consequently produce some changes in the active sites nature.

The crystalline domain size of cerium oxide was also calculated from the CeO_2 main signal of the corresponding Raman spectra, as proposed by Kanakaraju et al. [27]. The results indicate a size of 2.8, 4.1 and 4.6 nm for NiCe (0.11)–PA, NiCe (0.17)–PA and NiCe (0.25)–PA, respectively. The values are lower than those estimated by the Scherrer equation; however they follow an identical trend. These differences could be explained by structural defects [28].

On the other hand, several sectors of two catalytic papers (NiCe (0.11)–PA and NiCe (0.17)–PA) were analyzed by EDX technique in order to get further insights about distribution of the active phases. The Ce/Ni atomic ratios were, in general, close to the expected values. In the case of NiCe (0.11)–PA sample the average ratio was 0.12 ± 0.035 and that for NiCe (0.17)–PA was 0.16 ± 0.036. These

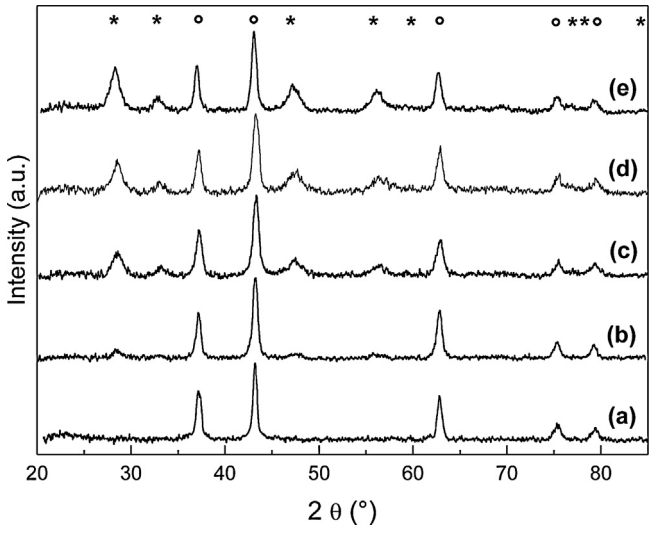

Fig. 4. X-ray diffraction patterns of the catalysts: Ni–PA (a), NiCe (0.05)–PA (b), NiCe (0.11)–PA (c), NiCe (0.17)–PA (d) and NiCe (0.25)–PA (e). Symbols: ◦NiO; *CeO_2.

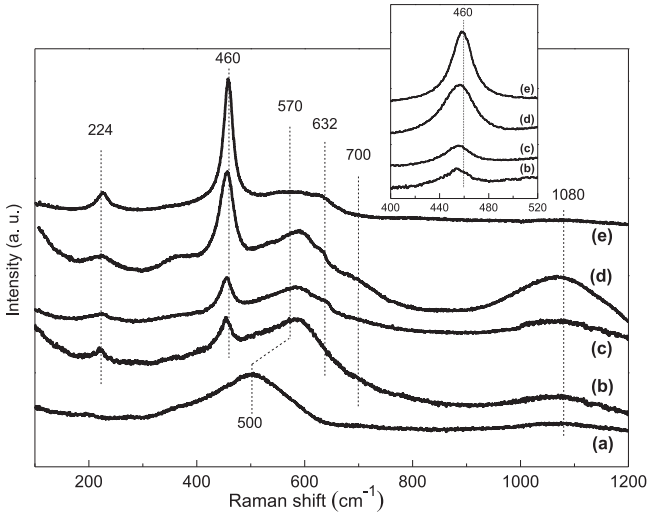

Fig. 5. Laser Raman spectra of the catalysts: Ni–PA (a), NiCe (0.05)–PA (b), NiCe (0.11)–PA (c), NiCe (0.17)–PA (d) and NiCe (0.25)–PA (e). Inset: main signal of cerium oxide for each catalyst (F2g mode).

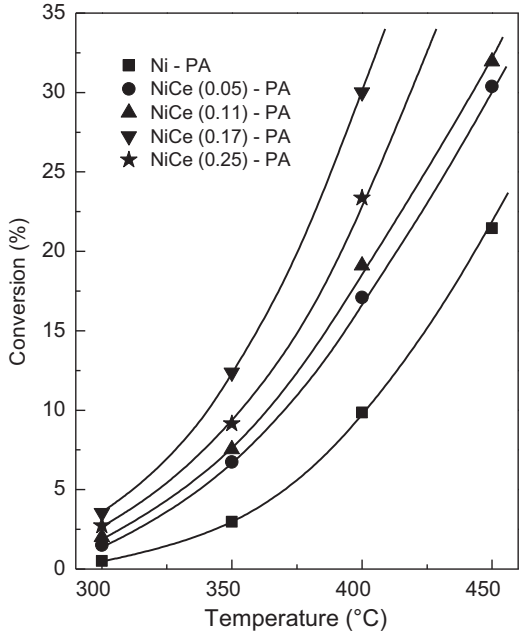

Fig. 6. Ethane conversion of the catalytic papers. Reaction conditions: $W/F = 0.08$ g s/cm^3, $C_2H_6/O_2 = 1$.

results show that the active components were spread reasonably well along the ceramic fiber structures, indicating a quite homogeneous distribution of the active phases. However, according to the irregular arrangement of the ceramic fibers a few sectors presented a low or high active components ratios.

3.3. Catalytic performance on the ethane oxydehydrogenation

Fig. 6 shows the ethane conversion in the range of the analyzed temperatures for the prepared catalysts. Bulk nickel oxide exhibits a high catalytic activity for the oxidative dehydrogenation of ethane. This system showed ethane conversion even at the lowest temperature. Nevertheless, the addition of cerium to the formulations notoriously increased the ethane conversion.

The incorporation of the promoter with a Ce/Ni = 0.17 atomic ratio increased the ethane conversion at 300 °C by a factor of seven while this increment was about three times at 400 °C. However, the addition of a higher amount of cerium (Ce/Ni = 0.25) produced a decrease in the catalytic activity, suggesting that there is an optimal Ce/Ni atomic ratio to achieve high activity.

Fig. 7 shows the selectivity to ethylene as a function of ethane conversion at 350 °C for the catalysts. Under the used reaction conditions, Ni–PA shows low selectivity to ethylene (~27%) while Ce-containing catalysts achieve higher values (38–45%), being the maximum value for NiCe (0.17)–PA.

The increment of the ethane conversion at a fixed temperature produced a very slight drop in the selectivity, which showed an almost flat tendency suggesting that the ethylene total oxidation was minimized. Therefore, carbon dioxide was mainly generated directly from ethane oxidation. It is worth mentioning that no carbon monoxide was measured in the products gas stream.

On the other hand, the observed increment in both ethane conversion and selectivity improved the ethylene productivity in cerium-promoted systems. At 400 °C, NiCe (0.17)–PA showed an ethylene production about six times higher than the Ni–PA sample. The same trend in the productivity was observed at all reaction temperatures (300 and 350 °C) (Fig. 8).

A ceramic paper without active phases (PA) was evaluated at the same reaction conditions as those of the catalytic papers. This

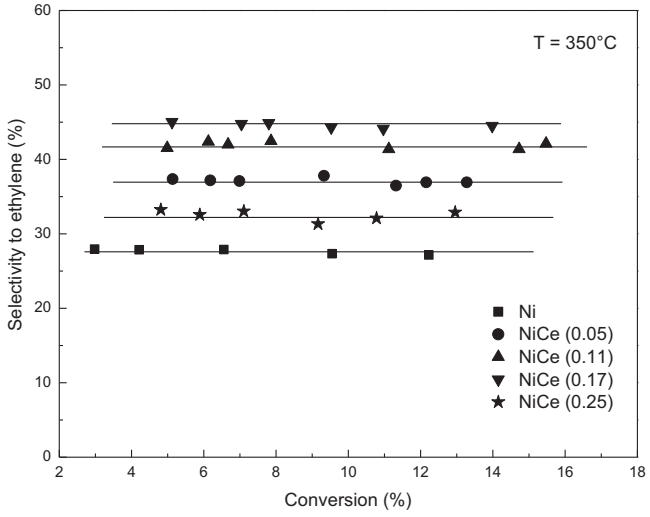

Fig. 7. Selectivity to ethylene of the catalytic papers. Reaction conditions: $T = 350$ °C, W/F = variable, $C_2H_6/O_2 = 1$.

system showed both negligible ethane conversion and selectivity even at 450 °C and thus no ethylene productivity, indicating that no active species for the oxidative dehydrogenation reaction were present in the original substrate.

A careful investigation by scanning electron microscopy was performed to assess the stability of the catalysts. Several micrographs were taken after submitting the catalytic papers to the reaction conditions during more than 20 h. The results (not shown) indicated that the alumina layer presents a very high stability onto the alumina–silica fibers after the catalytic tests. No layer detachments were observed after analyzed numerous sectors. At the same time, the catalytic particles remains unchanged (shape and morphology) and well adhered to the ceramic fibers, indicating an adequate adherence of the active phases to the network structure.

In summary, the system NiCe (0.17)–PA showed the best ethane conversion and selectivity and hence the highest ethylene productivity. This behavior could be explained by the presence of the smallest crystalline domain size of nickel oxide (XRD) and the partial incorporation of nickel cation into the ceria lattice, which lead to generating new active sites for the reaction (LRS).

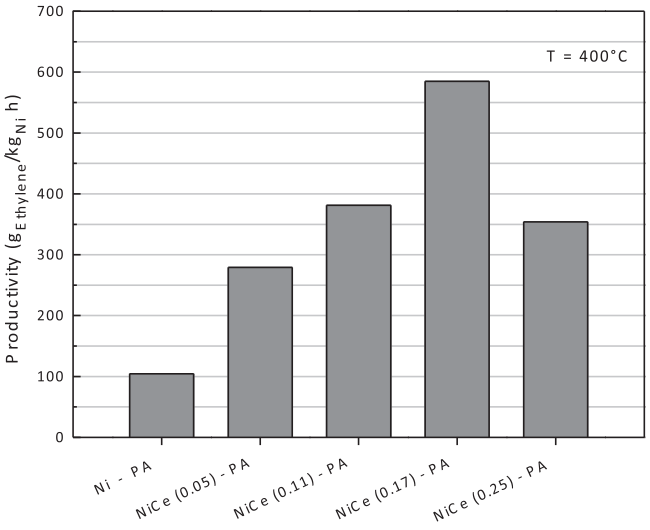

Fig. 8. Ethylene productivity of the catalytic papers at 400 °C ($g_{ethylene}/kg_{Ni}$ h).

4. Conclusions

Ceramic papers have an interconnected fibers structure, covered by nanometric alumina particles. This arrangement constitutes an adequate environment for the dispersion of catalysts and allows a stable deposition of a catalytic formulation.

Catalytic ceramic papers exhibit nickel oxide as active phase (XRD, LRS) and show a very high activity for the ODE reaction. The presence of Ce as promoter causes a decrease in the nickel oxide crystalline domain and induces modifications in the active sites nature, due to the partial incorporation of the Ni component into the ceria lattice. Thus, the catalytic performance is noticeably improved and ethylene productivity is markedly increased.

Even with a low amount of active phases (metal oxides) these structured systems show high ethylene production, demonstrating that they are a promising topic for further development. The control of selectivity through modifications in the preparation process and the catalytic formulations constitute an interesting challenge.

Acknowledgements

The authors wish to acknowledge the financial support received from ANPCyT (Grant PME 87-PAE 36985 to purchase the RAMAN Instrument), CONICET and UNL. Thanks are also given to Elsa Grimaldi for the English language editing.

References

[1] T. Granato, F. Testa, R. Olivo, Microporous and Mesoporous Materials 153 (2012) 236–246.
[2] L.F. Bobadilla, A. Álvarez, M.I. Domínguez, F. Romero-Sarria, M.A. Centeno, M. Montes, J.A. Odriozola, Applied Catalysis B: Environmental 123–124 (2012) 379–390.
[3] M.A. Ulla, R. Mallada, L.B. Gutierrez, L. Casado, J.P. Bortolozzi, E.E. Miró, J. Santamaría, Catalysis Today 133–135 (2008) 42–48.
[4] J.P. Bortolozzi, L.B. Gutierrez, M.A. Ulla, Applied Catalysis A: General 452 (2013) 179–188.
[5] Y. Matatov-Meytal, M. Sheintuch, Applied Catalysis A: General 231 (2002) 1–16.
[6] H. Koga, T. Kitaoka, H. Wariishi, Journal of Materials Chemistry 19 (2009) 5244–5249.
[7] H. Koga, S. Fukahori, T. Kitaoka, M. Nakamura, H. Wariishi, Chemical Engineering Journal 139 (2008) 408–415.
[8] J.P. Cecchini, R.M. Serra, C.M. Barrientos, M.A. Ulla, M.V. Galván, V.G. Milt, Microporous and Mesoporous Materials 145 (2011) 51–58.
[9] S. Fukahori, H. Ichiura, T. Kitaoka, H. Tanaka, Environmental Science and Technology 37 (2003) 1048–1051.
[10] H. Koga, H. Ishihara, T. Kitaoka, A. Tomoda, R. Suzuki, H. Wariishi, Journal of Materials Science 45 (2010) 4151–4157.
[11] E.D. Banús, M.A. Ulla, M.V. Galván, M.A. Zanuttini, V.G. Milt, E.E. Miró, Catalysis Communications 12 (2010) 46–49.
[12] S. Fukahori, H. Koga, T. Kitaoka, A. Tomoda, R. Suzuki, H. Wariishi, Applied Catalysis A: General 310 (2006) 138–144.
[13] A. Gurbani, J.L. Ayastuy, M.P. González-Marcos, M.A. Gutiérrez-Ortiz, International Journal of Hydrogen Energy 35 (2010) 11582–11590.
[14] A. Trovarelli, F. Zamar, J. Llorca, C. de Leitenburg, G. Dolcetti, J.T. Kiss, Journal of Catalysis 169 (1997) 490–502.
[15] Y. Wang, A. Zhu, Y. Zhang, C.T. Au, X. Yang, C. Shi, Applied Catalysis B: Environmental 81 (2008) 141–149.
[16] M.M. Pakulska, C.M. Grgicak, J.B. Giorgi, Applied Catalysis A: General 332 (2007) 124–129.
[17] P. Boizumault-Moriceau, A. Pennequin, B. Grzybowska, Y. Barbaux, Applied Catalysis A: General 245 (2003) 55–67.
[18] Y.M. Liu, L.C. Wang, M. Chen, J. Xu, Y. Cao, H.Y. He, K.N. Fan, Catalysis Letters 130 (2009) 350–354.
[19] H. Koga, T. Kitaoka, in: D. Pozo Perez (Ed.), On-paper Synthesis of Silver Nanoparticles for Antibacterial Applications in Silver Nanoparticles, In-Tech, Croatia, 2010, pp. 277–294.
[20] SCAN Standard Methods SCAN-C 26:76 and SCAN-M 5:76.
[21] B. Solsona, P. Concepción, S. Hernández, B. Demicol, J.M. López Nieto, Catalysis Today 180 (2012) 51–58.
[22] M. Azhar Khan, M.U. Islam, M. Ishaque, I.Z. Rahman, A. Genson, S. Hampshire, Materials Characterization 60 (2009) 73–78.
[23] M. Prekajski, Z. Dohčević-Mitrović, M. Radović, B. Babić, J. Pantić, A. Kremenović, B. Matović, Journal of the European Ceramic Society 32 (2012) 1983–1987.
[24] W. Shan, M. Luo, P. Ying, W. Shen, C. Li, Applied Catalysis A: General 246 (2003) 1–9.
[25] N.M. Deraz, Ceramics International 38 (2012) 747–753.
[26] A. Martínez-Arias, M. Fernández-García, L.N. Salamanca, R.X. Valenzuela, J.C. Conesa, J. Soria, Journal of Physical Chemistry B 104 (2000) 4038–4046.
[27] S. Kanakaraju, S. Mohan, A.K. Sood, Thin Solid Films 305 (1997) 191–195.
[28] L. Bourja, B. Bakiz, A. Benlhachemi, M. Ezahri, S. Villain, C. Favotto, J.C. Valmalette, J.R. Gavarri, Powder Technology 215–216 (2012) 66–71.